ON THE INFLUENCE OF TRANSIENT AERODYNAMIC HEAVE VIBRATIONS ON RACING CAR SUSPENSION PARAMETERS: AERO POST RIG IN A QUARTER CAR TEST

AUTHORS:

Timoteo Briet Blanes

AERODYNAMICS RESEARCH GROUP

ABSTRACT:

Vehicles running at high speed are greatly influenced by their aerodynamic profile. Racing car teams strive to tune the setup seeking higher levels of downforce aerodynamic load. Wind tunnel tests or track data for specific vehicle positions are useful but incomplete and very expensive. Transient loads on the vehicle come from very different sources and, to date, there is no established methodology to take them into consideration. Computer simulation seems to be a good starting point to study the effect of transient aerodynamic loads in the design and optimization of the tuning of the suspension of a racing car.

This paper studies the effect of transient aerodynamic loads on the downforce of a vehicle. Heave vibrations on an aileron are analyzed on a simulation model. The data obtained in this simulation model are validated both in a steady and a transient state for different frequencies (1-800Hz). These results lead to the obtainment of a transfer function for the downforce on the aileron in question. Finally, a new quarter car model including aerodynamic effects from these studies is presented and some results on the influence of heave transient aerodynamics loads on a racing car are obtained.

KEYWORDS:

Unsteady vibration, suspension, damper, racing car, CFD, transient aerodynamics, heave vibrations, downforce.

NOMENCLATURE:

U_∞ = Air Velocity.
ρ = Air density.

μ = Air viscosity.
υ = Kinematic viscosity.
Cu = Chord wing profile.
S = Wing span.
Lo = Characteristic length.
L = Aerodynamic lift or downforce.
L(s) = Lift force in Laplace space.
L(t) = Lift force in time.
C_L = Lift coefficient.
A = Wing area (Cu·S).
α = Wing incidence angle.
τ = Shear stress.
Cf = Friction coefficient.
Δx = Smaller mesh cell size.
Δt = Time step.
Co = Courant number.
GR = GrowthRate.
FS = Stretching Factor.
S1 = Thickness first boundary layer.
g = Gravity acceleration.
P = Pressure.
f = Frequency.
Am = Amplitude.
C(k) = Theodorsen complex function.
k = Reduced frequency
y+ = Mesh quality parameter .
y = Vertical displacement.
m_s = Sprung mass.
m_u = Unsprung mass.
T = Vibration period.

1. INTRODUCTION:

The performance of a racing car (F1, GP2, LMP, endurance, etc.) is largely influenced by its aerodynamics. Racing teams try to improve the vehicle performance seeking higher levels of support or aerodynamic charge ("downforce"), applied in an optimal way. Lots of working hours are wasted by teams on wind tunnel tests and track data, with the substantial financial outlay that this implies. Wind tunnel tests are performed in aerodynamic stationary conditions with the car fixed in static configurations. However, the height or pitch of a car when racing changes continuously due to countless factors: roughness or undulations, track cambers, braking or acceleration maneuvers, changes in direction, pilot actions, direction and intensity fluctuations of the wind and downforce variations due to different speeds and trajectories along a circuit. All these factors cause suspension components to move, especially the sprung (chassis) and unsprung (wheels) masses. These movements, in turn, can cause aerodynamic fluctuations [14] which can lead to alterations in tire grip. When there is gap between input (vibrations coming from different causes) and output (vibrations of the vehicle itself) the aerodynamic stationary conditions and the static vehicle configuration become invalid. These transient effects change the dynamics of the system [15].

The roll, yaw, pitch and heave motions of the sprung mass affect both the downforce and the position of the center of pressure. The suspension is responsible for dealing with such movements, but in order to achieve maximum effectiveness in high-performance vehicles, it is necessary to consider unsteady aerodynamic effects.

In recent years, several authors have worked on the transient state of aerodynamics and its effects, shedding some light on the problem.

In [3], [5], [11] and [15], the effects of transient aerodynamic forces in car stability are studied. Joint CFD simulations and test in wind tunnels, show that the aerodynamic effect is transient and reduces the pitching resonance frequency of the sprung mass vehicle.

One of the phenomena studied is the "porpoising" effect that makes the vehicle suffer pitch oscillations of great amplitude, which affect vehicle dynamics in a nonlinear way.

In [6] and [15], variations of "lift" (C_L) and pitching moment (C_{MY}) coefficients are studied in a model of vehicle subjected to sinusoidal oscillations, both pitch and swing, for four different frequencies. The wind tunnel tests conducted with a simplified model of vehicle, known as "Ahmed model," show that both parameters vary in amplitude and phase shift (with respect to the sinusoidal oscillation) with frequency. Another model used is a Le Mans car type in order to show the difference between the behavior in a steady and a transient state. Based on the experimental results, a transfer function is built for a linearized model for transient aerodynamics.

In [2], [7], [8], [20] and [21], the influence of transient aerodynamics in the fast and high amplitude of small wing movement is studied. The idea is that the aerodynamic models used for flight control, based on assumptions of quasi-static conditions are valid for conventional aircraft. Also, it examines the aerodynamic effects of an inverted wing ground effect performing a vertical ("heave") sinusoidal movement at different frequencies.

In [9] and [14], the transient aerodynamics of the "Ahmed model," with moving seesaw ("heave") is examined with CFD simulations. Studies show that in variations in the coefficient of "lift" (C_L) and pitching moment coefficient (C_m) three effects occur that depend on the movement: contraction of flow (dependent on vertical displacement), relative incident angle changes flux (depending on vertical speed) and the effect of added mass (depending on the vertical acceleration). Both coefficient variations "lift" (C_L) and pitching moment coefficient (C_m) have phase delay with respect to the vertical displacement.

In [18] and [19], numerical models are studied to identify systems, also for low Reynolds numbers.

In [23] the damper of a car suspension is optimized with a "7 Post rig" test (4 posts for the 4 wheels and 3 posts to simulate the effects of aerodynamics). This analysis, used until now by all racing teams, includes static aerodynamic data from tests calculated in wind tunnels.

In this paper, a methodology that allows the introduction of the transient effects of aerodynamics in the study and determination of the suspension of a car is presented. In section 2, the modeling and simulation of the aileron is presented. The developed model is based on CFD simulation, where the aileron (at different angle incidences) is confronted with a horizontal steady flow at constant air speed, and being vibrated perpendicularly up and down in heave direction at different frequencies (from 1Hz to 800Hz). In section 3, Theodorsen’s transient analytic studies are particularized to the aileron used in section 2. The results obtained for the static and transient cases from these simulations are gathered and validated in section 4. In section 5, these results are included through the transfer function (which include the aerodynamic effects) in a newly presented quarter car model, where a test is run to show the impact of including the aerodynamic effects in the dynamic suspension behavior of a vehicle.

Finally, in section 6 some conclusions are drawn and some future development lines are presented.

2. COMPUTATIONAL SIMULATION:

2.1. AIRFOIL, MOTION AND ANGLE INCIDENCE

The study presented in this article focuses on the geometry of a wing with a NACA 63415 profile (Fig. 1). The reason for this choice is that it simply does not have a symmetrical profile; it tries to imitate as closely as possible the profiles used in motorsport, and there is test data available [17].

The digits that define the NACA "abcde" profiles stand for:

- **"a"** multiplied by 0.15 gives, at the ideal angle of attack, the theoretical optimum lift coefficient C_L .
- **"bc"**, divided by 2, is the distance of maximum curvature from the leading edge as % of the chord.
- **"de"** maximum thickness of the profile in % of the chord.

For example, for a 63415 profile: the lift coefficient is $C_L = 0.9$, the maximum curvature occurs at position 17% of the chord from the leading edge and width of maximum thickness is 15% the size of the chord.

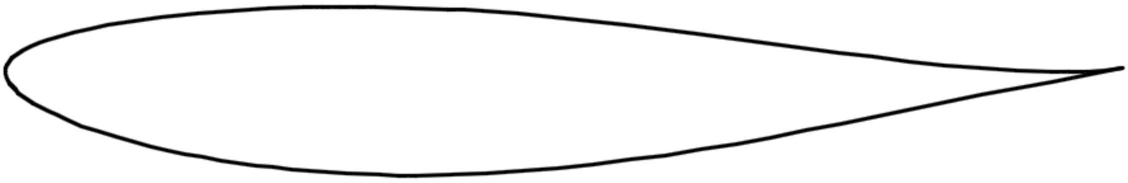

Figure 1. Profile NACA 63415

The span (perpendicular to profile) is 1 m, in order to calculate the forces per unit.

The computational simulation consists of two main parts. In the first one, the NACA profile is maintained static with a front wind of $U_\infty = 50$ m/s.

This allows the flow around the profile to stabilize after some time (simulations show that 0.25 s is enough for the stabilization to occur). Once a permanent and stable flow has been obtained, the profile is given an oscillatory movement, perpendicular to the wind direction, as shown in Fig. 2 (heave movement). The movement can vary in amplitude and frequency.

The vibration (Fig. 2) function that defines this movement is shown in Eq. (1), where the amplitude is called *Am* (in meters), the frequency is *f* (in Hz) and the time *t* (in seconds), starting at $t = 0.251$ s, just the next time step after the stabilization has been achieved ($\Delta t = 0.001$ s in the stabilization simulation):

$$y(t) = Am \cdot \sin\left(f \cdot (t - 0.251)\right) \qquad (1)$$

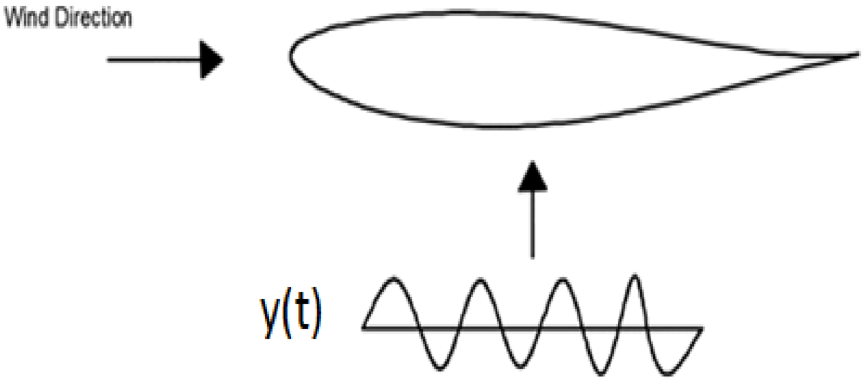

Figure 2. Vibration in wing

The frequencies chosen for the simulations are: 1Hz, 4Hz, 8Hz, 16Hz, 32Hz, 64Hz, 128Hz, 400Hz and 800Hz, which allows for a complete study of the behavior of the profile in a large frequency span (not covered so far, to the knowledge of the authors, in studies published to date.).

The amplitude has been chosen to vary linearly with the frequency between 0.0001 m (at 800Hz) and 0.048 m (at 1Hz).

The simulations also take into account three possible angles of attack "α" (Fig. 3) for the NACA profile. The first angle has been chosen to be 3.15º (TestS1), which is a common angle of attack for downforce in car competition; the other two simulations will be performed at angles of incidence of 6.15º (TestS2) and 9.15º (TestS3). The chord (Cu) of the profile has been chosen to be 0.241 m, also common in racing cars.

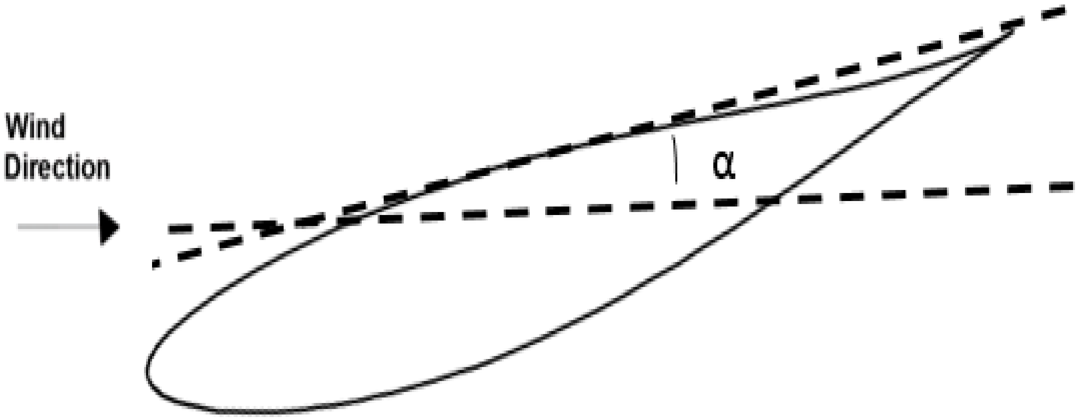

Figure 3. Angle of attack of NACA profile

2.2. SIMULATIONS CONDITIONS:

The computational simulation of a vibrating profile inside air flow can be represented by the Navier Stokes equations that in Gibbs formulation can be shown in Eq. (2) [25].

$$\rho\left(\frac{\partial v_x}{\partial t}+v_x\frac{\partial v_x}{\partial x}+v_y\frac{\partial v_x}{\partial y}+v_z\frac{\partial v_x}{\partial z}\right)=-\frac{\partial P}{\partial x}+\mu\left(\frac{\partial^2 v_x}{\partial x^2}+\frac{\partial^2 v_x}{\partial y^2}+\frac{\partial^2 v_x}{\partial z^2}\right)+\rho g_x$$

$$\rho\left(\frac{\partial v_y}{\partial t}+v_x\frac{\partial v_y}{\partial x}+v_y\frac{\partial v_y}{\partial y}+v_z\frac{\partial v_y}{\partial z}\right)=-\frac{\partial P}{\partial y}+\mu\left(\frac{\partial^2 v_y}{\partial x^2}+\frac{\partial^2 v_y}{\partial y^2}+\frac{\partial^2 v_y}{\partial z^2}\right)+\rho g_y$$

$$\rho\left(\frac{\partial v_z}{\partial t}+v_x\frac{\partial v_z}{\partial x}+v_y\frac{\partial v_z}{\partial y}+v_z\frac{\partial v_z}{\partial z}\right)=-\frac{\partial P}{\partial z}+\mu\left(\frac{\partial^2 v_z}{\partial x^2}+\frac{\partial^2 v_z}{\partial y^2}+\frac{\partial^2 v_z}{\partial z^2}\right)+\rho g_z$$

(2)

Being the continuity Eq. (3) of the problem:

$$\left(\frac{\partial v_x}{\partial x}+\frac{\partial v_y}{\partial y}+\frac{\partial v_z}{\partial z}\right)=0$$

(3)

To be able to vibrate the profile perpendicularly to the flow direction, and to calculate reliable and accurate values for downforce, simulation meshing must be able to adapt to the movement.

This can be achieved by a “morphing” mesh type. For this study the software STAR CCM + V8 CD-Adapco is used. The included "morphing-mesh" option can modify the initially created mesh to be able to adapt to the movement, that is, to compress and extend the mesh where it is needed.

This makes it necessary to create a fine initial mesh to reposition the aileron while it moves.

To be able to assure appropriate accuracy a base size geometry of 0.1 m has been selected.

The turbulence model chosen is the standard K-epsilon [26].

To generate the mesh of surrounding air, first a 2D mesh is created as shown in Fig. 4. Based on this mesh the 3D mesh extrude is created in the 1m deep profile.

The minimum length for this problem has been chosen to be 0.0005 m and the mesh target to 0.001 m.

These values control the general creation of the mesh for the profile and the air.

When the curvature of the geometry requires a finer mesh, the minimum value is selected.

These specific values are widely used to optimize calculation time at the same time that good accuracy is achieved. Fig. 4, 5 and 7 show a close up of the meshing.

Wind speed attacking the profile has been chosen to be constant during all the simulation at 50 m/s, which represents a commonly accepted reference speed for a racing car.

The surrounding air is considered to be at 20ºC, with the viscosity "μ" and the density "ρ" being constant since the speed corresponds to an incompressible state (< 100 m/s).

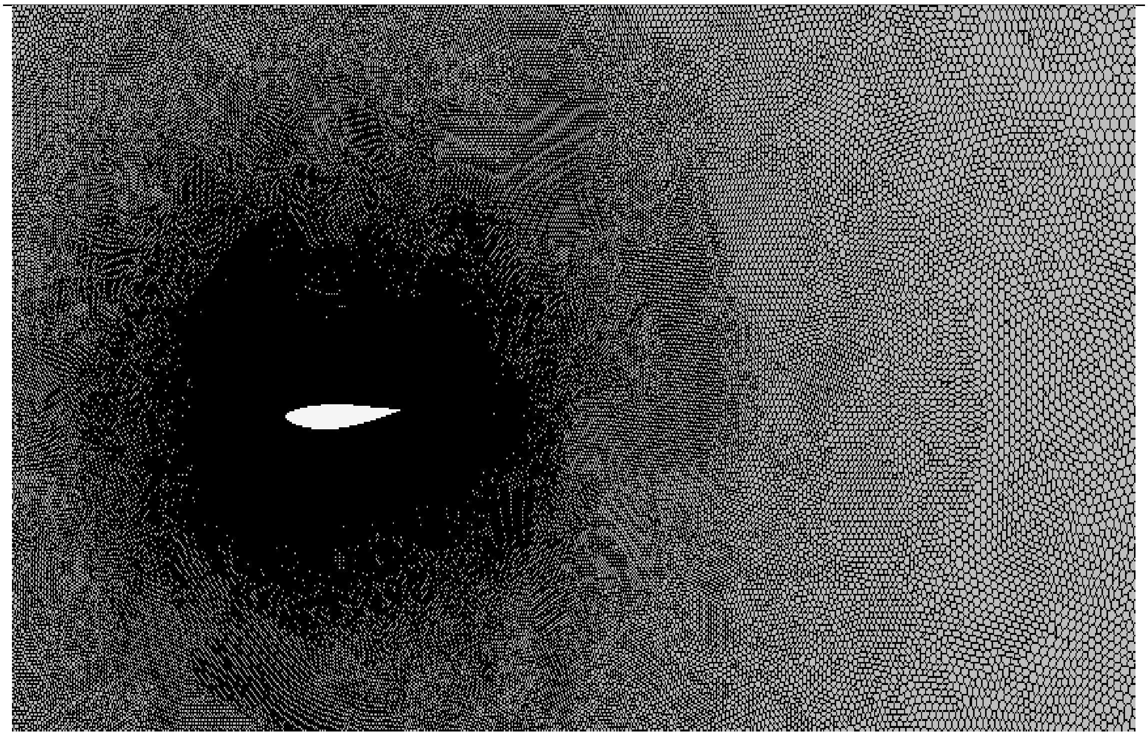

Figure 4. General mesh

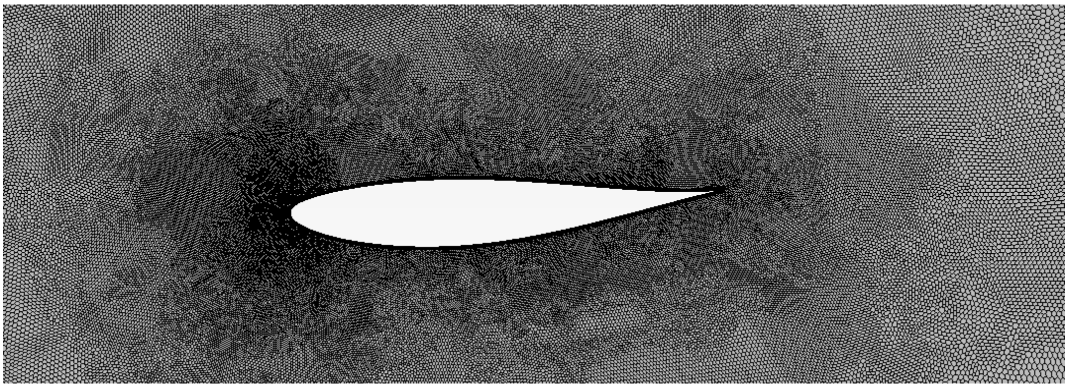

Figure 5. Profile mesh

The boundary layer is the area where the most important effects are produced from an aerodynamic point of view, defining the subsequent dynamics of the air. It is common practice to use a large number of boundary layers to obtain good results.

To do this, first the thickness of the first boundary layer S1, the most important, is calculated in Eq. (4). Mesh quality layer is defined by the *y*+ parameter. In this case, as the profile is simple enough, the best value for *y*+ can be chosen (*y*+ = 1) providing the best possible precision [16].

$$S1 = \frac{y^{+}\mu}{\sqrt{\dfrac{\dfrac{0.026}{\left(\dfrac{\rho U_{\infty} Cu}{\mu}\right)^{1/7}}\rho U_{\infty}^{2}}{2}}} \tag{4}$$

Applying the specific values of air density and viscosity, along with the *Cu* (chord and, in this example, characteristic length), *U* and *y+*, the thickness *S1* is obtained and equal to $6 \cdot 10^{-6}$ m. In order to improve calculation speed and accuracy, a relatively large number of boundary layers (10 layers) is selected.

Moreover, the "stretching" factor ("FS"), indicates the ratio of thicknesses of successive layers forming the limit layer. For example, in this case, for a "FS = 1.75" and 3 layers composing the boundary layer, the distribution of the boundary layers is shown in Fig. 6. In the NACA profile a FS of 1.75 has been selected for the 10 layers giving a boundary layer total thickness of 2 mm.

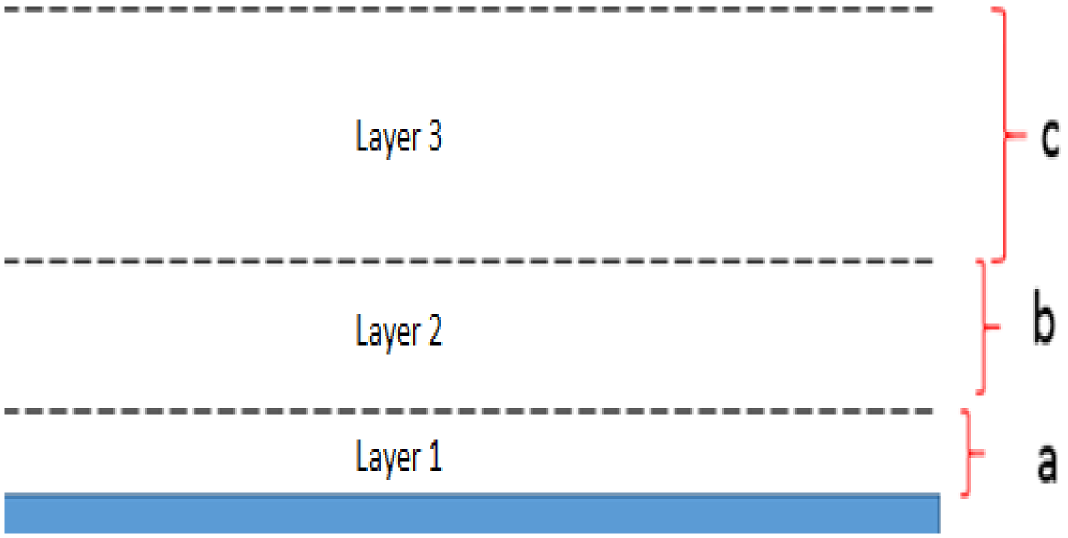

b =1.75 a   c = 1.75 b

Figure 6. Thickness sample between layers in boundary layer total

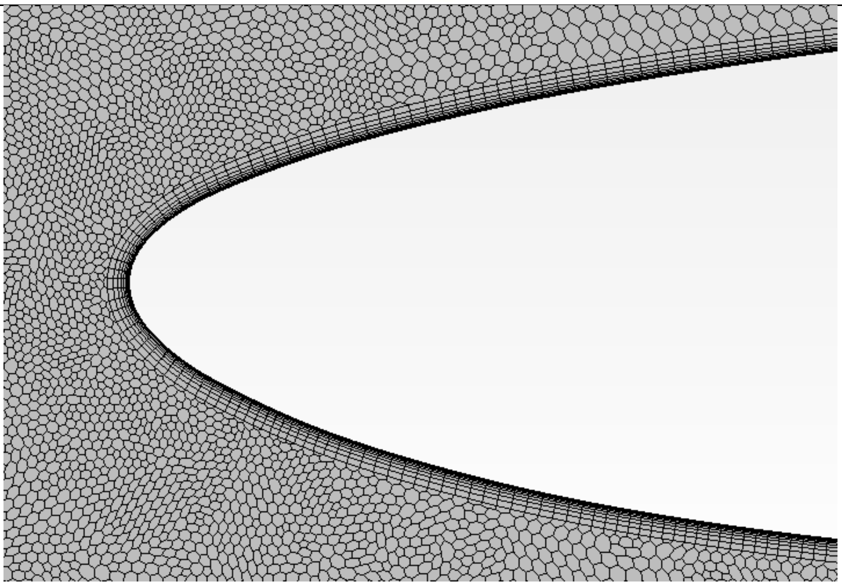

Figure 7. Mesh detail for boundary layers for NACA 63415

It is important to select a good “GrowthRate” (GR) of the global mesh. The GR is a measure of the adequacy of the density of the mesh. A sufficiently low GR value needs to be selected to make the simulation independent of the density of the mesh and, at the same time, to make it stable. In order to select the right GR value, a series of simulations have been carried out, making the mesh transition smooth. The result of such simulation is shown in Fig. 8, where the change in C_L is represented versus the GR value. In the graph it can be seen that for a GR value smaller than 1.21, the C_L value is stable. These simulations have been carried out for an incidence angle of 6.15º for TestS2 setup. For the sake of calculation accuracy and stability a GR value of 1.01 has been selected and kept fixed for all the setups and simulations. The mesh shown in Fig. 4, 5 and 7 have been created with a GR of 1.01.

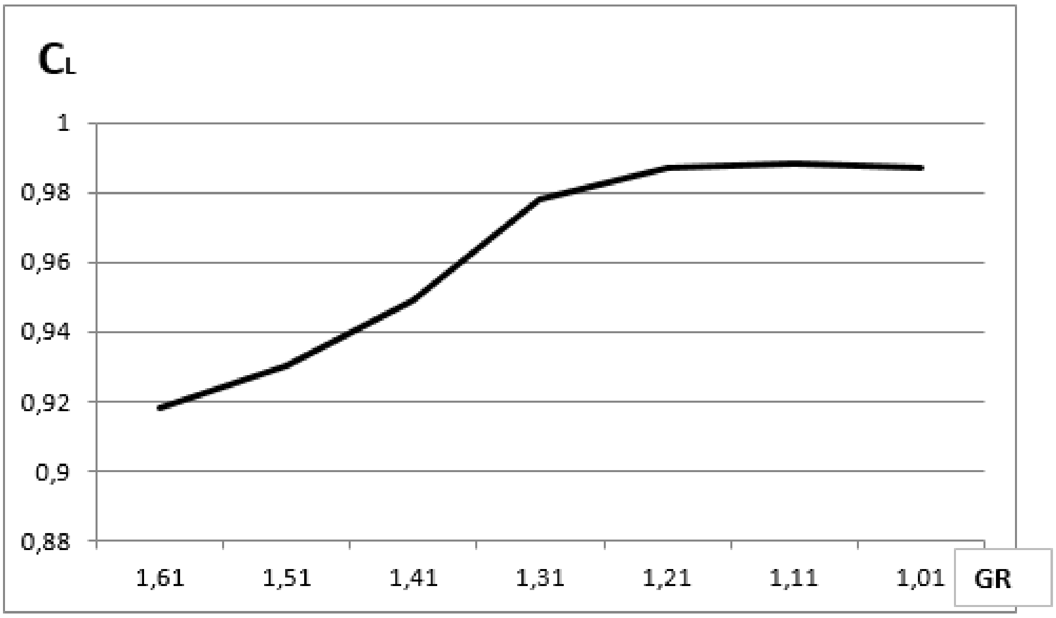

Figure 8. Lift coefficient in function of “GR” (TestS2)

In these simulations it is important to assure that for each time step all the mesh cells have been taken into account and not overseen. Failing to obtain this would lead to precision loss in cell calculation, which in turn would lead to a growing error at each following iteration.

Courant number in Eq. (5) is a value that quantifies the speed of iteration from cell to cell in an area of the mesh. In order to do this correctly a Courant number (*Co*) of 1 is chosen. The time step can be obtained from Eq. (5), being Δx the minimum mesh size and being $U(x)$ the wind speed at position (x). In this paper a Δt of 0.0001 s is obtained.

$$Co = \frac{\Delta t}{\frac{\Delta x}{U(x)}} = \frac{U(x)\Delta t}{\Delta x} \tag{5}$$

2.3. SIMULATION RESULTS

As mentioned, the computation simulation is divided in two different parts. The first, in which the aileron is kept static and the flow is stabilized around it after some time. Once this happens, the aileron is forced to follow an oscillatory pattern. One typical result of such CFD simulations is shown in Fig. 9. In this figure, the calculated downforce on the profile is depicted. There it is possible to distinguish two different parts in the graph. The first one, under 0.25s, where the flow and the downforce are stabilized (part A and B in the figure). Then, at exactly 0.251 s, the vibration starts, and the oscillatory downforce on the aileron becomes evident (part C).

In particular, Part A in Fig. 9 corresponds to the time interval between the start of the simulation and the convergence. Part B allows the convergence to stabilize and, once this occurs, Part C accounts for the downforce calculation at the oscillation of the aileron. It can be seen that between parts B and C an abrupt jump exists, that corresponds to an initial and fast computational instability in the transition from a static permanent position to a transient one.

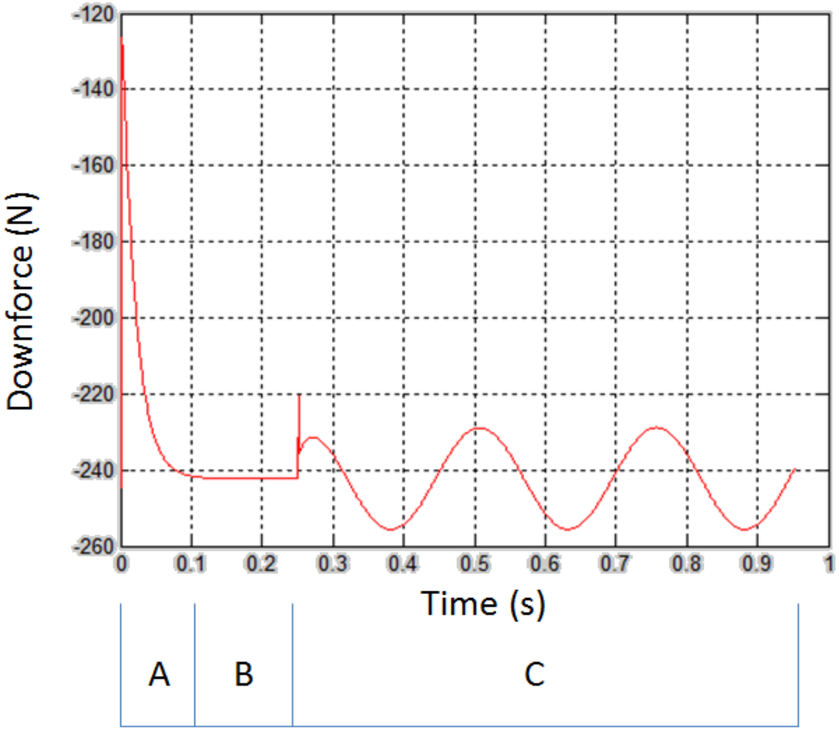

Figure 9. Convergence, stabilization and unsteady vibration in simulation example

In this paper the CFD simulation has been run for the NACA 63415 profile, at a constant front wind speed, for three different angle incidences (TestS1 3.15º, Test S2 6.15º and TestS3 9.15º) at nine different frequencies (1Hz, 4Hz, 8Hz, 16Hz, 32Hz, 64Hz, 128Hz, 400Hz and 800Hz).

For each frequency, the amplitude of the vibration is fixed.

The downforce values after stabilization (Part B in Fig. 9) are the following:

TestS1	245.23 N
TestS2	371.05 N
TestS3	471.41 N

Table 1. Stabilized downforce

In all these simulations it is possible to identify a clear linear pattern between input (imposed input) and output (calculated downforce).

Therefore it is possible to analyze both, input and output, to get a gain (relation between the amplitudes of both signals) and a phase angle (delay in the output signal).

In Fig. 10-12, as an example, both, input and output signals, have been shown for specific frequencies.

For example, in Fig. 10, both signals are shown for a 4Hz frequency, at a 3.15º (TestS1) angle of attack.

The graph shows the downforce in ordinates on the left, and the position of the aileron in mm on the right.

From the comparison of both signals a gain and offset can be calculated.

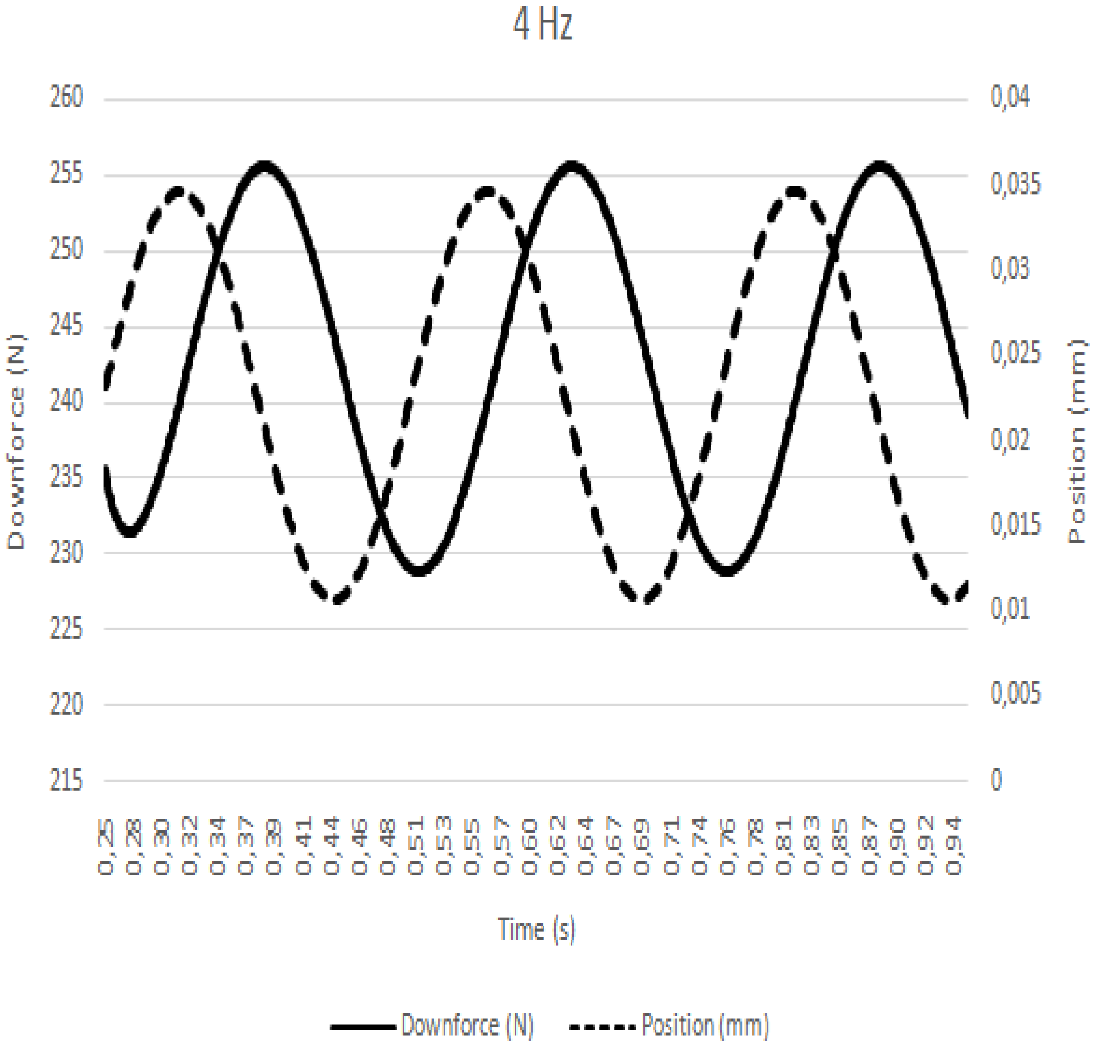

Figure 10. Input and output at 4 Hz for TestS1

A similar situation can be seen in Fig. 11, where a 64Hz input signal is in place at a 6.15º angle of attack (TestsS2).

It can be seen that the difference between peaks in both signals (offset) is different from that in Fig. 10.

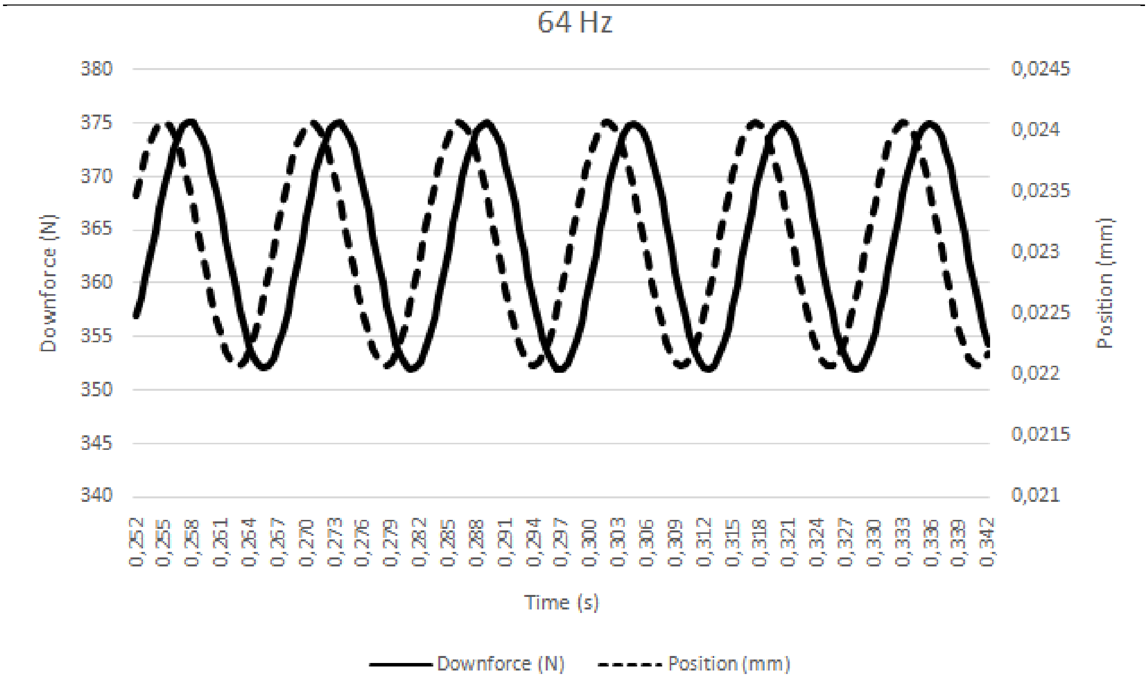

Figure 11. Input and output at 64 Hz for Test S2

In Fig. 12, at 800Hz input signal is shown at a 6.15º angle of attack (TestsS3). Again, the phase between both signals is different.

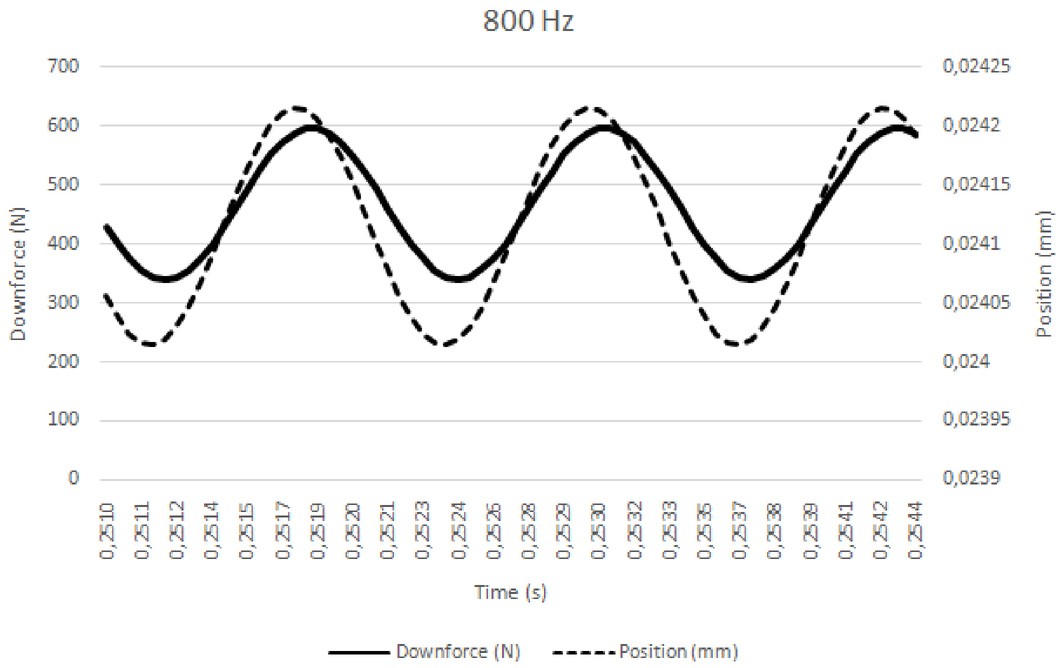

Figure 12. Input and output at 800 Hz for Test S3

The output signal from the simulation can be adjusted to follow a sine function. In order to obtain the amplitude and phase between both signals, Eq. (6) for input signal, and Eq. (7) for downforce signal can be used.

$$y_i(t) = y_{m,i} + Am_{0,i} \cdot \sin\left(f_i \cdot t + \phi_{h,i}\right)$$

(6)

$$L_i(t) = L_{m,i} + L_{0,i} \cdot \sin\left(f_i \cdot t + \phi_{L,i}\right)$$

(7)

Where $y_i(t)$ is the sine input for the position of the aileron and $L_i(t)$ the downforce corresponding to the output frequency f_i; $Am_{0,i}$ y $L_{0,i}$ are the amplitudes and $\Phi_{h,i}$, $\Phi_{L,i}$, the phases. y_{mi} and $L_{m,i}$, are average values. The process used to calculate the bode plot and thus the transfer function is shown next.

Once ratio of amplitudes and phase are calculated for input and output signal for all frequencies, it is possible to build a transfer function for the given problem. In general, there are two signals, as shown in Fig. 13.

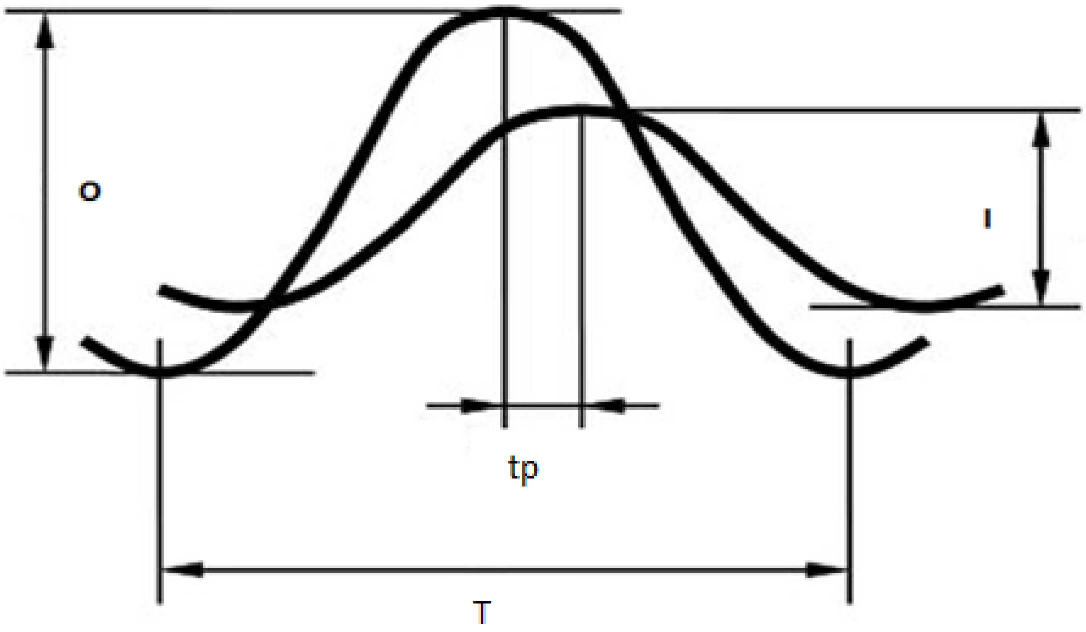

Figure 13. Input and Output general signals

For a given frequency of oscillation f_i the amplitude is obtained in decibels as shown in Eq. (8).

$$Am_{dB(i)} = 20 \cdot \log_{10}\left(\frac{O}{I}\right) = 20 \cdot \log_{10}\left(\frac{L_{0,i}}{Am_{0,i}}\right)$$

(8)

And the phase angle in degrees as:

$$\varphi_i = \frac{360 \cdot tp}{T} = \left(\phi_{L,i} - \phi_{h,i}\right) \cdot \frac{180}{\pi}$$

(9)

This procedure has been repeated for all the tests and the transfer function between both signals can be constructed in a bode plot. The results are shown in Tables 2-4.

For TestS1 in α=3.15º angle of incidence:

$f_i[Hz]$	$Am_{0,i}[m]$	$\phi_{L,i}-\phi_{h,i}[^\circ]$	$L_{0,i}[N]$	α=3.15º
1	0.04	1.57	11.7	
4	0.012	4.557	13.370	
8	0.006	8.066	11.850	
16	0.003	8.114	9.730	
32	0.0019	4.183	9.732	
64	0.001	1.193	11.530	
128	0.0005	13.348	18.700	
400	0.0002	43.580	66.120	
800	0.0001	132.050	131.900	

Table 2. Results for 3.15º

For TestS2 in α=6.15º angle of incidence:

$f_i[Hz]$	$Am_{0,i}[m]$	$\phi_{L,i}-\phi_{h,i}[^\circ]$	$L_{0,i}[N]$	α=6.15º
4	0.012	1.650	12.530	
8	0.006	1.759	11.640	
16	0.003	8.078	9.413	
32	0.0019	7.833	9.626	
64	0.001	5.155	11.530	
128	0.0005	5.421	18.560	
400	0.0002	31.18	65.600	
800	0.0001	0.097	131.000	

Table 3. Results for 6.15º

For TestS3 in α=9.15º angle of incidence:

$f_i[Hz]$	$Am_{0,i}[m]$	$\phi_{L,i}-\phi_{h,i}[^\circ]$	$L_{0,i}[N]$	α=9.15º
4	0.012	1.562	10.900	

8	0.006	1.668	10.24
16	0.003	1.688	8.778
32	0.0019	1.508	9.599
64	0.001	7.383	11.47
128	0.0005	7.136	18.190
400	0.0002	25.416	64.500
800	0.0001	75.96	129.000

Table 4. Results for 9.15º

Applying Eqs. (8) and (9) to these results, the values shown in Table 5 are obtained:

	α=3.15º		**α=6.15º**		**α=9.15º**	
Frequency	*Amplitude* (dB)	*Phase (º)*	*Amplitude (dB)*	*Phase (º)*	*Amplitude (dB)*	*Phase (º)*
1 Hz	49.02	-90.83				
4 Hz	60.939	-98.896	60.375	-89.490	59.165	-94.543
8 Hz	65.911	-102.148	65.756	-95.610	64.643	-100.825
16 Hz	70.22	-104.910	69.932	-87.890	69.328	-102.835
32 Hz	74.189	-89.392	74.094	-81.290	74.097	-88.798
64 Hz	81.237	-68.354	81.237	-63.010	81.184	-64.640
128 Hz	91.457	-44.784	91.392	-48.390	91.217	-49.4
400 Hz	110.386	-23.050	110.317	-16.240	110.171	-13.518
800 Hz	122.405	-5.910	122.345	-12.090	122.212	-5.558

Table 5. Bode plot points

These values can be shown in a bode plot:

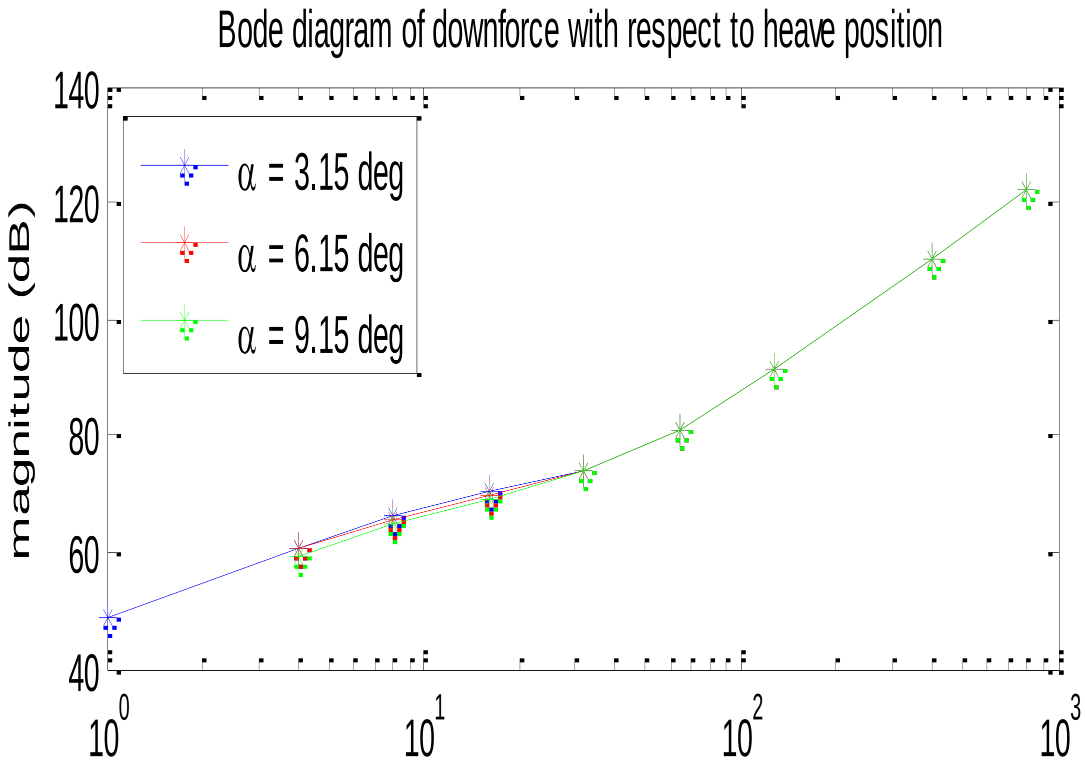

Figure 14. Bode diagram magnitude

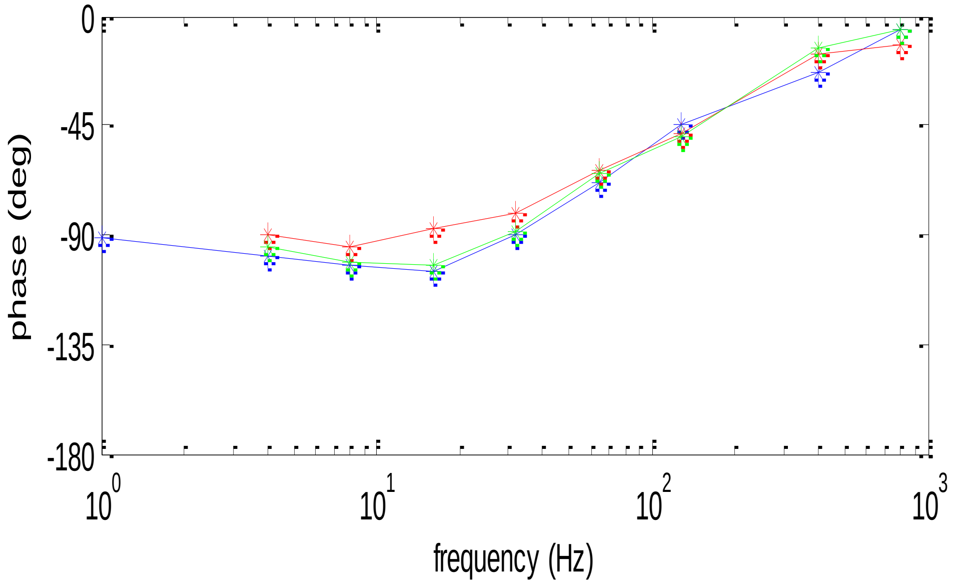

Figure 15. Bode diagram phase

From Fig. 14 it can be seen that amplitude does not depend on the angle of incidence of the profile. However, it can be seen that in Fig. 15 the phase angle shows slight differences between them at specific frequencies.

3. TRANSIENT ANALYTIC STUDY

Simulations obtained in section 2 show results in permanent and transient situations. These computational results are validated in section 4. Stable flow around a given profile can be easily compared to its wind tunnel results. Validation of the transient part is more complicated. On the one hand, usually there is no test data available for these transient conditions and, on the other hand, it is difficult to obtain it. Notwithstanding this, some analytical theories do exist that can be consulted to validate transient aerodynamic data.

In this paper, the fundamental development of Theodorsen [1] in the field of unsteady aerodynamics has been used to validate the obtained results. In this section Theodorsen offers a theory to represent lift and pitch moments for small harmonic oscillations for a thin plate working inside an incompressible flow. This theory is a common point of reference for studies working with transient aerodynamics [10] [12] [13].

Theodorsen [1] proposes that the *y(t)* heave position can be normalized, dividing it by the chord of the airfoil (*Cu*). At the same time, the time can also be normalized by the ratio between the chord and the speed of the flow (U_∞):

$$y^* = \frac{y}{Cu}; \qquad t^* = \frac{t}{\frac{U_\infty}{Cu}} = \frac{t \cdot Cu}{U_\infty}$$

(10)

Under these premises, the velocities and accelerations can be normalized as:

$$\dot{y}^* = \frac{dy^*}{dt^*} = \frac{d\left(y\frac{1}{Cu}\right)}{d\left(t\frac{U_\infty}{Cu}\right)} = \frac{1}{U_\infty}\frac{dy}{dt} = \frac{1}{U_\infty}\dot{y}$$

(11)

$$\ddot{y}^* = \frac{d\dot{y}^*}{dt^*} = \frac{d\left(\dot{y}\frac{1}{U_\infty}\right)}{d\left(t\frac{U_\infty}{Cu}\right)} = \frac{Cu}{U_\infty{}^2}\frac{d\dot{y}}{dt} = \frac{Cu}{U_\infty{}^2}\ddot{y}$$

(12)

The lift for a heave movement can be expressed as follows [2]:

$$L = \frac{\pi}{4} \cdot \rho \cdot Cu^2 \cdot \ddot{y} + \pi \cdot \rho \cdot Cu \cdot U_\infty \cdot \dot{y} \cdot C(k)$$

(13)

The relation between the lift and the lift coefficient C_L is given by Eq. (14) [22], considering 1 meter wing span:

$$\mathrm{L} = \frac{1}{2} \rho \cdot Cu \cdot 1 \cdot C_L \cdot U_\infty^2$$

(14)

The lift coefficient can be obtained:

$$C_L = \frac{\pi}{2} \frac{Cu}{U_\infty^2} \ddot{y} + 2\pi \frac{1}{U_\infty} \dot{y} C(k)$$

(15)

And applying Eqs. (11) and (12), it can be rewritten as:

$$C_L = \frac{\pi}{2} \ddot{y}^* + 2\pi \dot{y}^* C(k)$$

(16)

In Eqs. (15) and (16) C(k) represents the Theodorsen function, *k* being the reduced frequency, a dimensionless figure giving the number of oscillations made by the wing during the interval of time it takes the flow to travel along the chord length multiplied by *π*. Its expression is:

$$k = k_r \cdot \omega \qquad k = \frac{Cu \cdot \omega}{2 \cdot U_\infty} = k_r \cdot \omega \qquad (17)$$

where omega is the circular frenquency.

Usually *k* gives useful information about the range of unsteadiness that the system is suffering. It is usually accepted [4] that a value of *k < 0.05* represents a system with quasi-steady aerodynamics. When *k* is bigger than 0.05 the system is considered to be unsteady aerodynamics, and when *k > 0.2*, it is considered highly unsteady. It is important to know that the range of selected frequencies in this paper covers all three posibilites. Thus, frequencies 1Hz to 3Hz can be considered quasi-steady, from 4Hz to 32Hz the system is working in an unsteady condition and, finally, for frequencies from 64Hz to 800Hz the system is highly unsteady.

According to [4] *C(k)* is a complex function that can be approximated to:

$$C(k)=1-\frac{0.165}{1-\frac{a_1}{k}\cdot j}-\frac{0.335}{1-\frac{a_2}{k}\cdot j} \tag{18}$$

Where a_1 and a_2 depend on the value of *k*:

$$\mathrm{a}_1=0.045;\mathrm{a}_2=0.30;\text{ for } k<0.5$$
$$\mathrm{a}_1=0.041;\mathrm{a}_2=0.32;\text{ for } k\geq 0.5$$

Operating the complex Eq. (18), substituting *k* and making *j=s* the Eq. (19) is obtained:

$$C(k)=1-\frac{0.165\cdot k_r\cdot s}{k_r\cdot s+a_1}-\frac{0.335\cdot k_r\cdot s}{k_r\cdot s+a_2}$$

(19)

Unifying everything in a single term:

$$C(k)=\frac{0.5k_r^2s^2+(0.665a_1+0.835a_2)k_rs+a_1a_2}{k_r^2s^2+(a_1+a_2)k_rs+a_1a_2}$$

(20)

And applying the values of a_i to the Eq. (20):

$$C(k)=\frac{0.5k_r^2s^2+0.280425k_rs+0.01350}{k_r^2s^2+0.345k_rs+0.01350}\quad\text{for } k<0.5$$

(21)

and

$$C(k)=\frac{0.5k_r^2s^2+0.294465k_rs+0.01312}{k_r^2s^2+0.361\cdot k_rs+0.01312}\quad\text{for } k\geq 0.5$$

(22)

Eqs. (21) and (22) are graphed in Fig. 16.

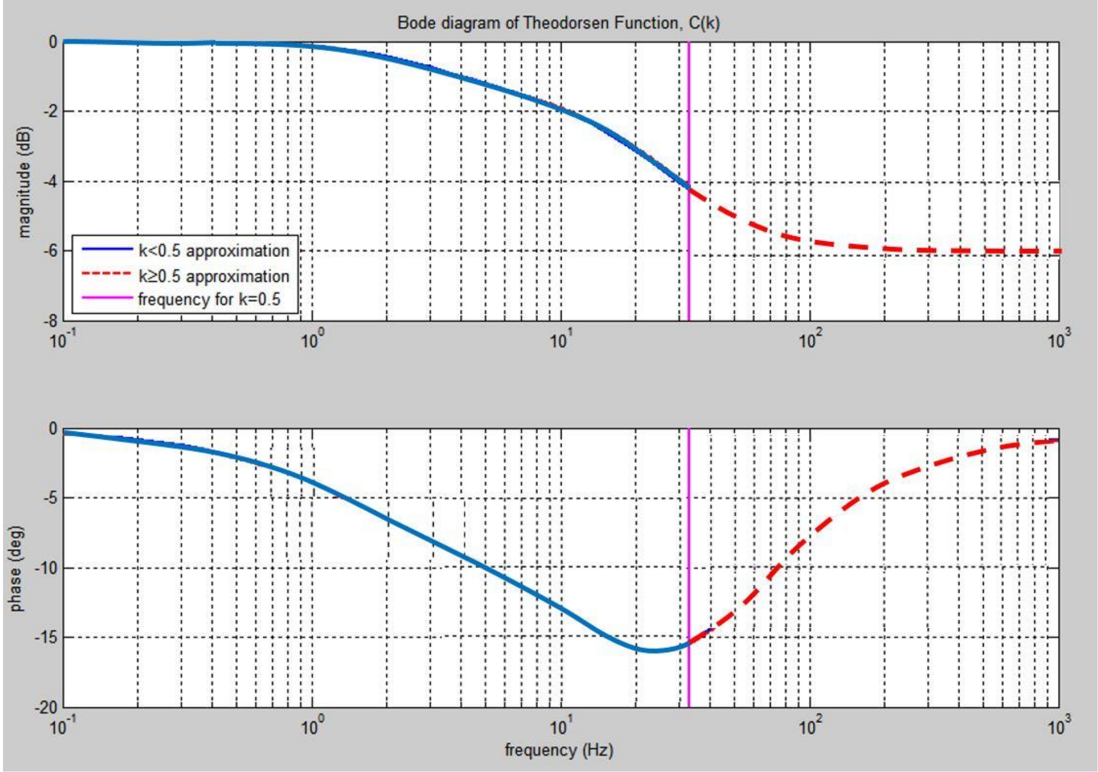

Figure 16. C(k) Bode plot

Applying the Laplace transformation to lift in Eq. (13) and dividing it by the Laplace transformation for acceleration and position of the profile the following transfer functions are obtained:

$$L(s) = \frac{\pi}{4} \cdot \rho \cdot Cu^2 \cdot s^2 Y(s) + \pi \cdot \rho \cdot Cu \cdot U_\infty \cdot s \cdot Y(s) \cdot C(k) \tag{23}$$

By dividing everything by Y(s) the following transfer function can be obtained between downforce and position on the profile:

$$\frac{L(s)}{Y(s)} = H_p(s) = \frac{\pi}{4} \cdot \rho \cdot Cu^2 \cdot s^2 + \pi \cdot \rho \cdot Cu \cdot U_\infty \cdot s \cdot C(k) \tag{24}$$

The transfer function between downforce L(s) and profile acceleration $s^2Y(s)$ can also be obtained:

$$\frac{L(s)}{s^2 Y(s)} = H_a(s) = \left[\frac{\pi}{4} \cdot \rho \cdot Cu^2 + \pi \cdot \rho \cdot Cu \cdot U_\infty \cdot \frac{1}{s} \cdot C(k) \right] s^2 \tag{25}$$

Figures 17-20 show graphically the transfer functions in Eqs. (24) and (25).

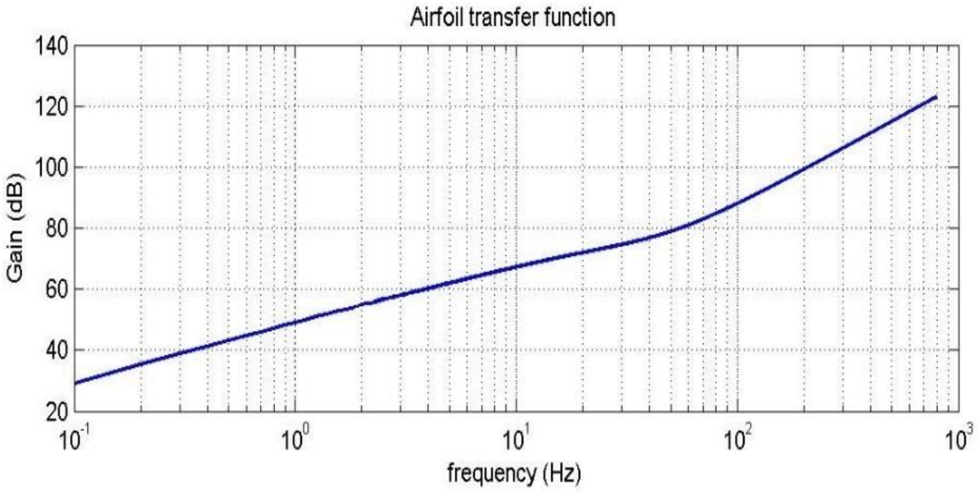

Figure 17. Downforce vs airfoil position gain

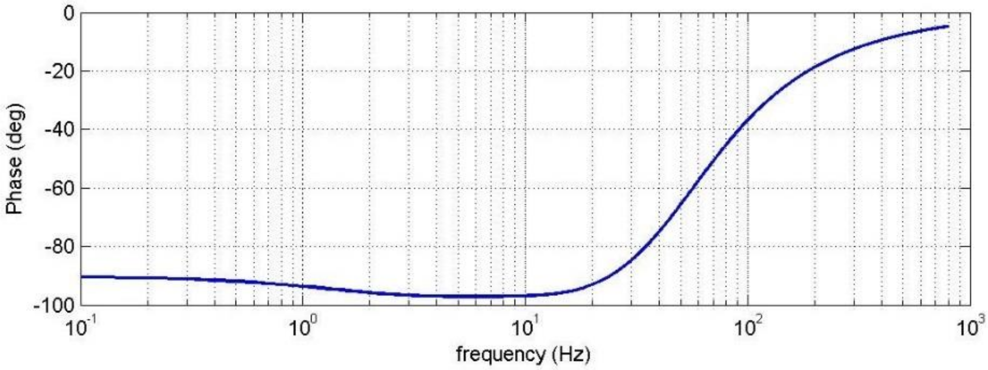

Figure 18. Downforce vs airfoil position phase angle

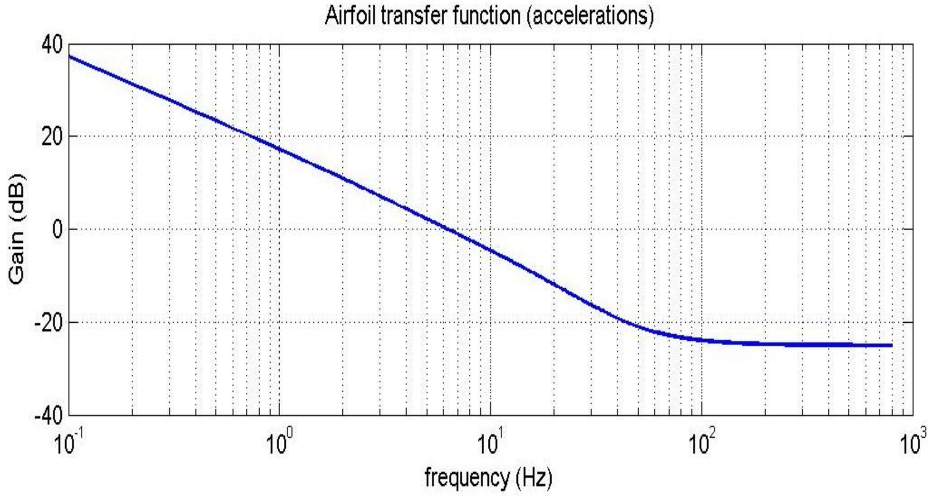

Figure 19. Downforce vs airfoil acceleration gain

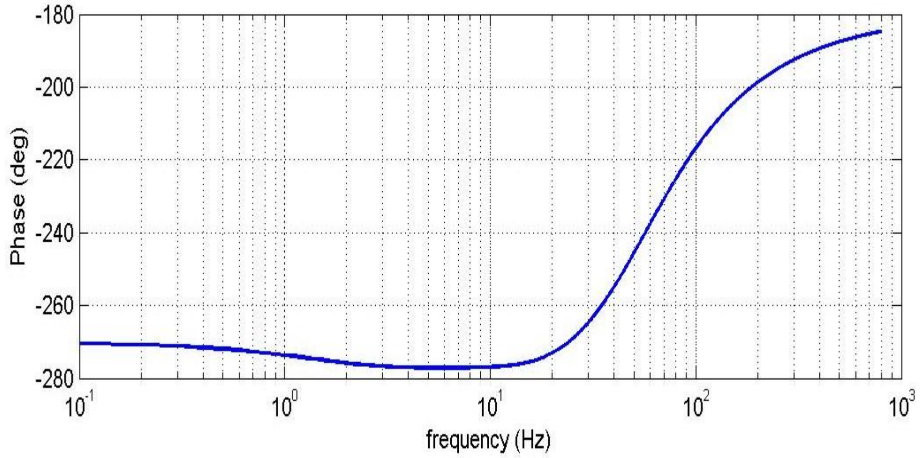

Figure 20. Downforce vs airfoil acceleration phase angle

4. VALIDATION RESULTS

4.1. STEADY AERODYNAMICS: (Zone AB in Fig. 9)

The results obtained in the simulations (section 2) need validation. On the one hand, steady flow around the static airfoil (zones A and B in Fig. 9) can be compared to wind tunnel results for the NACA 63415 profile that have been published [17]. On the other hand, the transfer functions developed in section 3 in the frequency space can serve as a reference to validate unsteady results in the CFD simulations and validate the model and methodology.

For the steady state validation, C_L values for different incidence angles for NACA 63415 profile, obtained in wind tunnel tests, are available in [17]. In Table 6, some values have been retrieved to compare them to the three incidence angles used in this study (3.15º, 6.15º and 9.15º); the values calculated are for a 850.000 Reynolds number:

Angle αº	C_L
3	0,6966
3,25	0,7249
6	1,0185
6,25	1,0392
9	1,2385
9,25	1,2521

Table 6. C_L values for interesting incidence angles for NACA 63415 profile

Results for steady state downforce were shown in Table 1, from which a C_L value can be obtained.

These values can be compared to the interpolation of the right incidence angles values in Table 6. In Table 7 both C_L values (from CFD simulations and wind tunnel tests) are compared. This table shows the error is greater for the smaller incidence angle and smaller for the bigger one, but it also shows that the proposed CFD model is quite close to reality.

Indicence angle	Downforce (N)	C_L - CFD	C_L – Wind tunnel	Error
3.15º	245.23	0.66	0.709	7.26 %
6.15º	371.05	0.99	1.026	3.71 %
9.15º	471.41	1.26	1.243	1.29 %

Table 7. C_L from Wind Tunnel test and CFD test

4.2. UNSTEADY AERODYNAMICS

So far the transfer function for CFD simulations in section 2 (Fig. 14-15) and the transfer function from the Theodorsen theory (Fig. 17-20) have been obtained. At this point both results are compiled in Fig. 21 and Fig. 22 to validate the model for the unsteady conditions. The red dots correspond to the CFD tests. It can be seen that, on the one hand, points obtained from the CFD model for different frequencies lay exactly on the Theodorsen curve in amplitude. For the phase angle graph it can be seen that there are some differences for frequencies between 64Hz and 800Hz,

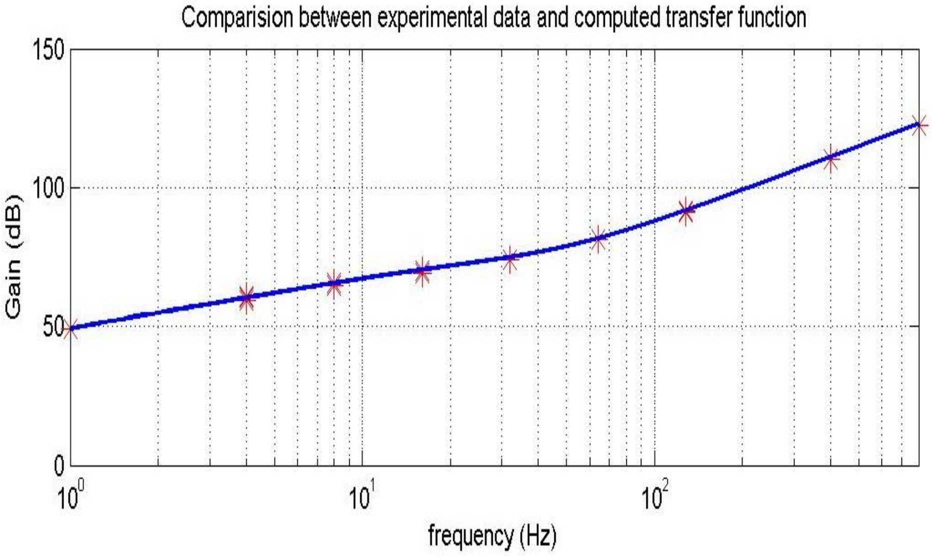

Figure 21. Bode plot gain comparison

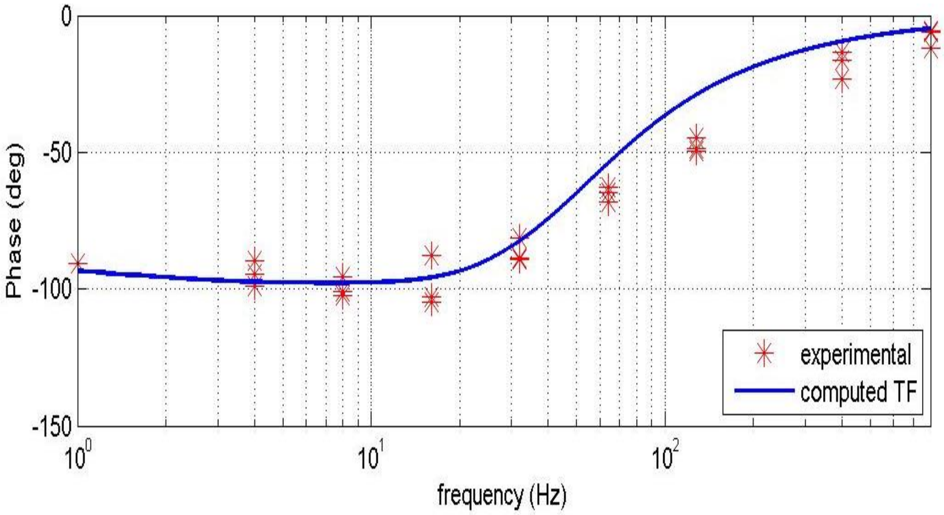

Figure 22. Bode plot phase angle comparison

In Fig. 23-24 the distribution of errors in amplitude and phase angle for the CFD simulation are shown. In amplitude, the relative error between simulation and analytical study is usually lower than 8%. Errors in phase angle are larger for high frequencies. These differences in phase angle for high frequencies can be explained by the fact that the Theodorsen theory takes into account thin plates and not specific profiles as in the CFD simulations. This deviation is more evident when the system is a high unsteadiness state.

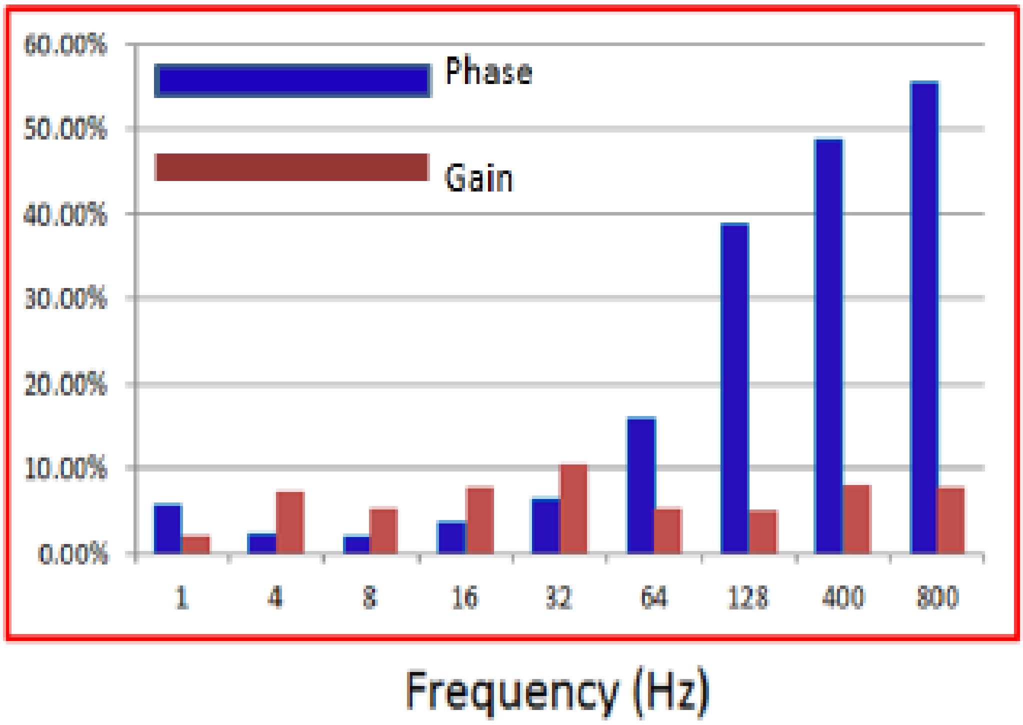

Figure 23. Gain error CFD vs Theodorsen

Figure 24. Phase angle error CFD vs Theodorsen

All in all, it can be concluded that the presented CFD model is good enough to represent amplitudes for a highly unsteady flow in a high frequency range. Besides, the model is also valid to represent phase angles for frequencies up to 64Hz. Higher frequencies reveal greater differences between simulation and the Theodorsen analytical study. As this study is based on thin plates and not on the actual NACA profile used in the CFD study, the suitability of the CFD model for frequencies higher than 64Hz remains unknown and would need further studies and validation in field tests. Apart from this uncertainty for higher frequencies, in general, the CFD models behave very well and its transfer function can be used for further studies, as the one shown in next section.

5. APPLICATION: RACING CARS SUSPENSION PARAMETER CALCULATION

In previous sections the effect of heave vibrations on an aileron and a transfer function for transient downforce have been studied. In real applications, e.g. vehicles with an airfoil, the unsteady downforce coming from the aerodynamic profile is normally transferred to its support, and from there to the car suspension and, finally to the tires. There are many fields where this study can be of interest. In this paper the focus has been put on racing cars.

In a racing car, aerodynamic downforce is directly transmitted to the vehicle chassis and, through it, to the suspension, allowing for a better grip between the tire and the road. In this system it is important to realize that the design of suspension is vital in order to make the best use of the transient forces in the car. In this section the previous results (transfer functions) are applied to a specific example for a racing car.

The overall problem is quite complicated, even for powerful racing car teams, due to the different load cases that might be present on the track. To take into account the aerodynamic effects on the car (if the racing team can afford it) wind tunnel tests can be carried out. However, even in this case transient effects are often overseen due to the difficulty of taking them into account, and static aerodynamic forces are only considered.

In this paper a first step forward is taken in order to start considering transient loads in the calculation of suspension parameters. The first objective in this simple application study is to start learning how transient aerodynamic forces are related to suspension parameters and, in turn, what should be taken into account for a future more comprehensive analysis. Subsequent subsections analyze this problem. In section 5.1 two simplified car models are presented, both of them representing a quarter of a car. One of these models includes, as a novelty, a representation of static or transient aerodynamic forces in the system. A further simplification of the problem considers that only heave vibrations are taken into account (considering negligible for example pitch vibrations). For this application a transfer function is obtained for the chassis position of both models. In section 5.2 data for a racing car is presented to copper-fasten and have some basic numeric data to evaluate the results in this study. In section 5.3, three methodologies to adjust the suspension parameters are presented. Two of them follow state of the art methods to calculate them, and the third presents a novel methodology to include transient aerodynamics in the system.

5.1. SIMPLIFIED CAR MODELS

Car behavior depends on the response of its suspension to outer inputs, such as road changes and/or aerodynamic forces. Traditional vehicle suspensions are comprised of two main components: springs and dampers. Spring characteristics (mainly preloads, lengths and hardness) are determined by the static weight of the vehicle and transfer loads for turns, accelerations, breakings and front-rear stability against pitch movements (e.g. caused by road bump instability).

The damper, in turn, is responsible for absorbing the vibrations and oscillations caused by the road or the external loads (e.g. aerodynamic forces) springs and tires, damping them out. The right selection of spring and dampers for a given application depends on the final application. In racing cars, the selection depends on the specific race track, the top speeds achievable in different parts of the track, and the magnitude of the instabilities that affect the car: turns, driver style, track oscillations, circuit rumble strips and aerodynamic downforce influence, among others.

The suspension in cars can be modeled by different simplified models. The quarter car model is one of the most useful (and more used) models of a vehicle's suspension which represents one corner of the suspension of the car [24]. The quarter car model shown in Fig. 25 depicts a typical suspension without any aerodynamic influence at all. Besides, it is important to note that this model is limited in that it is not possible to use it to study the longitudinal or lateral behavior of the car. However, this model is good enough (with a slight modification Fig. 26) for a first study of the influence of aerodynamic downforce on car suspension.

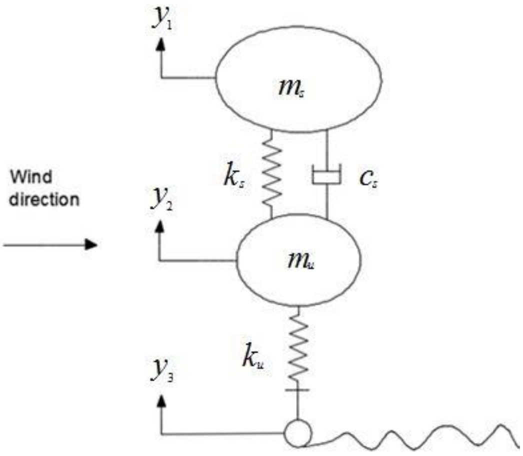

Figure 25. Quarter car model

In this model the tire is represented by a spring (k_u) and the suspension system as a spring (k_s) and a damper (c_s). Sprung mass in the car is represented by "m_s" and unsprung mass by "m_u".

The system movement follows the following differential equations:

$$m_s\ddot{y}_1 + c_s(\dot{y}_1 - \dot{y}_2) + k_s(y_1 - y_2) = 0$$
$$m_u\ddot{y}_2 + c_s(\dot{y}_2 - \dot{y}_1) + (k_s + k_u)y_2 - k_s y_1 = k_u y_3$$

(26)

Applying now the Laplace transformation:

$$\left(m_s s^2 + c_s s + k_s\right)\cdot Y_1(s) - \left(c_s s + k_s\right)\cdot Y_2(s) = 0$$

$$\frac{-\left(c_s s + k_s\right)}{k_u}\cdot Y_1(s) + \frac{\left(m_u s^2 + c_s s + k_s + k_u\right)}{k_u}\cdot Y_2(s) = Y_3(s)$$

(27)

Arranging the equation in matrix form:

$$\begin{bmatrix} m_s s^2 + c_s s + k_s & -c_s s - k_s \\ \dfrac{-\left(c_s s + k_s\right)}{k_u} & \dfrac{\left(m_u s^2 + c_s s + k_s + k_u\right)}{k_u} \end{bmatrix} \begin{Bmatrix} Y_1(s) \\ Y_2(s) \end{Bmatrix} = \begin{Bmatrix} 0 \\ 1 \end{Bmatrix} Y_3(s)$$

(28)

Comparing the input *$Y_3(s)$* with the outputs in *$Y_1(s)$* and *$Y_2(s)$* the following transfer functions are obtained:

$$F_1(s) = \frac{Y_1(s)}{Y_3(s)},\ F_2(s) = \frac{Y_2(s)}{Y_3(s)}$$

(29)

Where *$F_1(s)$* and *$F_2(s)$* represent the transfer function of the position of the sprung and unsprung mass vs the position of the road.

$$\begin{bmatrix} m_s s^2 + c_s s + k_s & -c_s s - k_s \\ \dfrac{-\left(c_s s + k_s\right)}{k_u} & \dfrac{\left(m_u s^2 + c_s s + k_s + k_u\right)}{k_u} \end{bmatrix} \begin{Bmatrix} F_1(s) \\ F_2(s) \end{Bmatrix} = \begin{Bmatrix} 0 \\ 1 \end{Bmatrix}$$

(30)

$$\begin{Bmatrix} F_1(s) \\ F_2(s) \end{Bmatrix} = \begin{bmatrix} m_s s^2 + c_s s + k_s & -c_s s - k_s \\ \dfrac{-\left(c_s s + k_s\right)}{k_u} & \dfrac{\left(m_u s^2 + c_s s + k_s + k_u\right)}{k_u} \end{bmatrix}^{-1} \begin{Bmatrix} 0 \\ 1 \end{Bmatrix}$$

(31)

Solving the equation, the final transfer functions for *$F_1(s)$* and *$F_2(s)$* are obtained:

$$F_1(s)=\frac{k_u\left(c_s s+k_s\right)}{m_u m_s s^4+\left(m_u c_s+m_s c_s\right)s^3+\left(m_u k_s+m_s k_s+m_s k_u\right)s^2+c_s k_u s+k_s k_u}$$

$$F_2(s)=\frac{k_u\left(m_s s^2+c_s s+k_s\right)}{m_u m_s s^4+\left(m_u c_s+m_s c_s\right)s^3+\left(m_u k_s+m_s k_s+m_s k_u\right)s^2+c_s k_u s+k_s k_u}$$

(32)

The suspension model in Fig. 25 does not include any aerodynamic load. However, for racing cars this aerodynamic downforce is very important, as it helps the tire to have more grip. Therefore, as a novelty, a new suspension model is now proposed. This model includes, as part of the sprung mass, the aerodynamic airfoil, as shown in Fig. 26. The transfer function for this airfoil has been validated in previous sections.

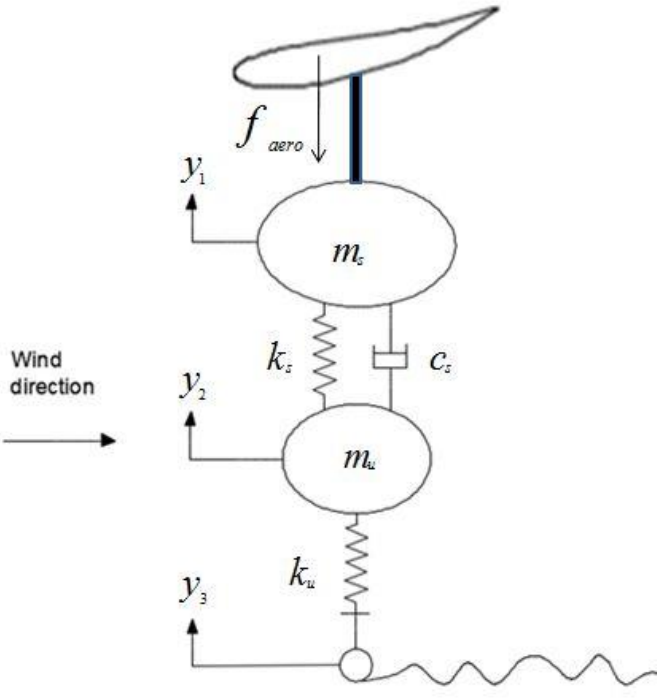

Figure 26. Quarter car model with aerodynamic forces

In this case the equations of the model in Fig. 26 are:

$$\begin{aligned} m_s\ddot{y}_1+c_s\left(\dot{y}_1-\dot{y}_2\right)+k_s\left(y_1-y_2\right)&=-f_{aero}\\ m_u\ddot{y}_2+c_s\left(\dot{y}_2-\dot{y}_1\right)+\left(k_s+k_u\right)y_2-k_s y_1&=k_u y_3 \end{aligned}$$

(33)

Applying Laplace transform:

$$\left(m_s s^2 + c_s s + k_s\right)\cdot Y_1(s) - \left(c_s s + k_s\right)\cdot Y_2(s) = -F_{aero}(s)$$

$$\frac{-\left(c_s s + k_s\right)}{k_u}\cdot Y_1(s) + \frac{\left(m_u s^2 + c_s s + k_s + k_u\right)}{k_u}\cdot Y_2(s) = Y_3(s)$$

(34)

The position transfer function *H(s)* of the downforce of the aileron has been obtained in section 3 in Eq. (24) and applied to this model in Eq. (35).

$$H(s) = \frac{F_{aero}(s)}{Y_1(s)} \Rightarrow F_{aero}(s) = H(s)\cdot Y_1(s)$$

(35)

Substituting the result in Eq. (34):

$$\left(m_s s^2 + c_s s + k_s\right)\cdot Y_1(s) - \left(c_s s + k_s\right)\cdot Y_2(s) = -H(s)\cdot Y_1(s)$$

$$\frac{-\left(c_s s + k_s\right)}{k_u}\cdot Y_1(s) + \frac{\left(m_u s^2 + c_s s + k_s + k_u\right)}{k_u}\cdot Y_2(s) = Y_3(s)$$

(36)

Reordering the terms and putting the equations in matrix form:

$$\begin{bmatrix} m_s s^2 + c_s s + k_s + H(s) & -c_s s - k_s \\ \dfrac{-\left(c_s s + k_s\right)}{k_u} & \dfrac{\left(m_u s^2 + c_s s + k_s + k_u\right)}{k_u} \end{bmatrix} \begin{Bmatrix} F_1(s) \\ F_2(s) \end{Bmatrix} = \begin{Bmatrix} 0 \\ 1 \end{Bmatrix}$$

(37)

Inverting the matrix and solving the system equation, the new $F_1(s)$ and $F_2(s)$ transfer functions are calculated for this new model:

(38)

$$F_1(s)=\frac{k_u(c_s s+k_s)}{m_u m_s s^4+(m_u c_s+m_s c_s)s^3+(m_u H(s)+m_u k_s+m_s k_s+m_s k_u)s^2+(c_s H(s)+c_s k_u)s+(k_s H(s)+k_s k_u+k_u H(s))}$$

$$F_2(s)=\frac{k_u\left(m_s s^2+c_s s+k_s+H(s)\right)}{m_u m_s s^4+(m_u c_s+m_s c_s)s^3+(m_u H(s)+m_u k_s+m_s k_s+m_s k_u)s^2+(c_s H(s)+c_s k_u)s+(k_s H(s)+k_s k_u+k_u H(s))}$$

5.2. RACING CAR DATA EXAMPLE:

In order to get some idea of the influence of the aerodynamic loads on a quarter car suspension model example, the following data is applied to the equations.

- Sprung mass: 40 kg
- Unsprung mass: 8 kg
- Wheel stiffness: 15.000 N/m
- Suspension stiffness: 2.000 N/m
- Damper coefficient of the suspension: 1.200 N/m*s

The suspension model will be tested with a step function of 10 mm of amplitude. This sudden change in road position will serve to study the dynamics of the system with and without aerodynamics.

5.3. QUARTER CAR MODEL RESULTS:

At this point it is now possible to compare the behavior of the model with and without aerodynamic influence. There are different methods to evaluate the dynamic response of a system. In this case a simple step function is used. This function simulates that the road has a permanent change of 10 mm upwards from one moment on. Once the height change on the road is in place, the quarter car model reacts to it. The reaction of the system depends on all the variables of the model and one can study the influence of each of these parameters in the final response, allowing for fine tuning of any of the objective parameters (normally the selection of the damper coefficient – or suspension setup – in a racing car).

The results of this study can show how the position of the airfoil (sprung mass) or the tire deflection change in time. In Fig. 27 the sprung mass position, after the 10 mm height change occurs, is shown for both models.

From the curves in the figure, it is clear that an evident influence of aerodynamics exists. On the one hand, it can be seen that aerodynamic forces make the system react quicker (a lesser period of time Ta < Ts between consecutive peaks in the signal). On the other hand, the movement of the sprung mass includes an extra dampening due to the aerodynamic effects. The maximum amplitude of the step response in the aerodynamic model is around 8% smaller than in the non-aerodynamic one.

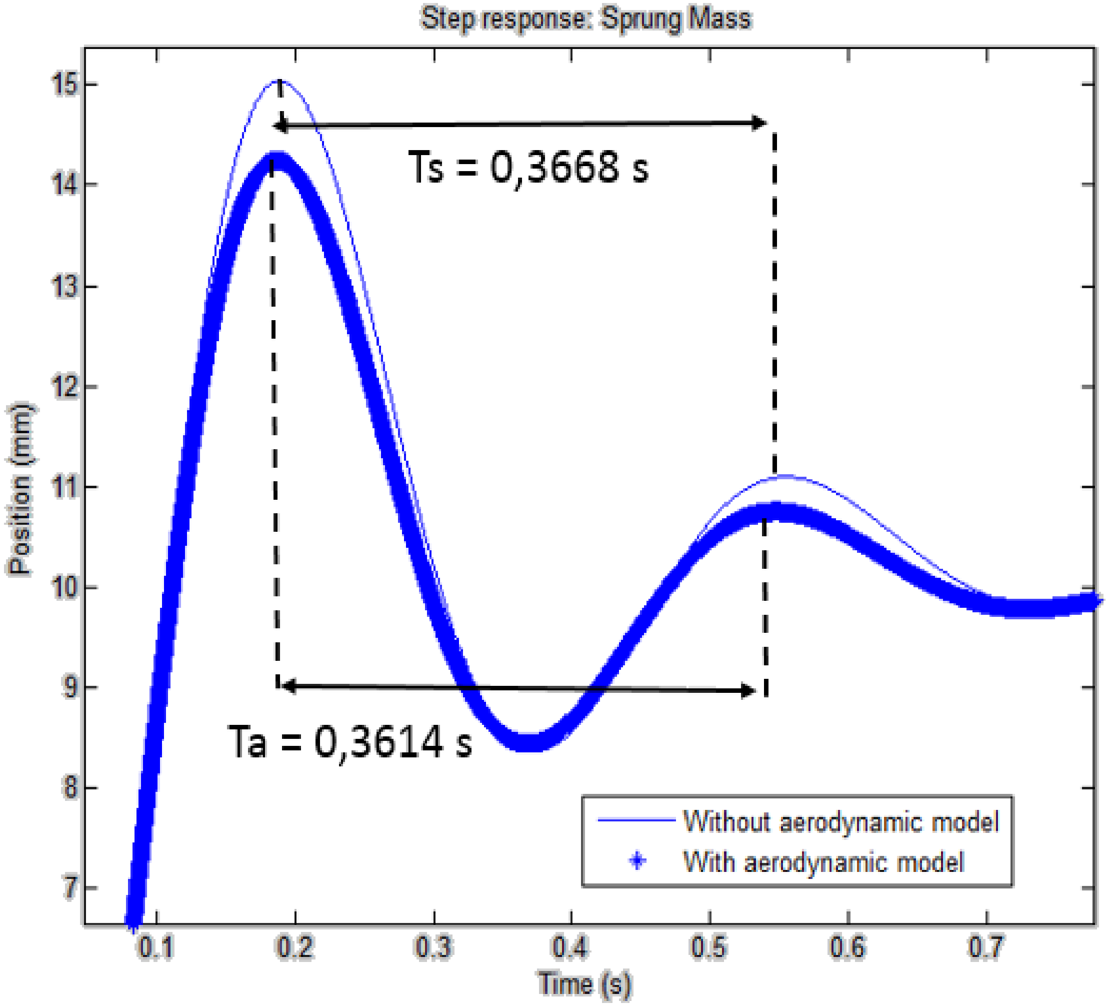

Figure 27. Time response sprung mass

It is also possible to study the tire deflection where similar results can be observed (Fig. 28).

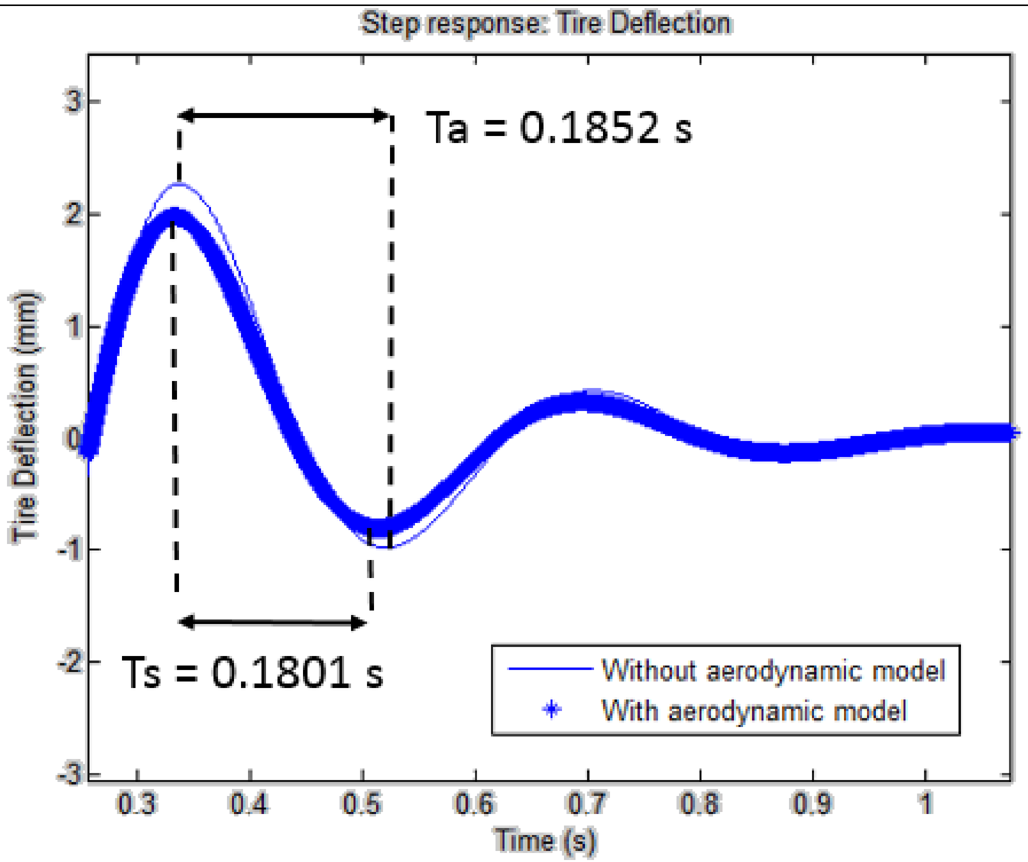

Figure 28. Time response "Tire deflection"

6. ACKNOWLEDGEMENTS

The author would like to acknowledge the support of my family.

7. CONCLUSIONS AND FUTURE DIRECTIONS

This paper deals with the study and the influence of heave vibrations in aerodynamic downforces. A transient aerodynamic CFD model for a range of frequencies for a heave movement between 1Hz and 800Hz and different pitch angles has been presented for a NACA 63415 airfoil.

The model has been successfully validated for aerodynamic stationary conditions and also for transient conditions. It has been shown that a transfer function between heave movement frequencies and airfoil downforce can be obtained for this problem and a methodology has been developed to achieve it.

An innovative quarter car model has been presented to take into account transient aerodynamic forces in car suspensions.

This improved quarter car model can be used to optimize the calculation of car suspension parameters in different working conditions.

Further studies will include, on the one hand, the study of the influence of pitch vibrations and combined pitch and heave vibrations. On the other hand, the quarter car model including aerodynamic forces can be generalized, for example, to a half-car bicycle model. Following steps will include the study of overall vibrations for all 3D degrees of freedom (pitch, yaw, roll or heave) and/or the generalization to a full car model.

8. REFERENCES:

[1] T. Theodorsen and W. Mutchler, "General theory of aerodynamic instability and the mechanism of flutter," vol. 496, pp. 413–433, 1935.

[2] J. Molina and X. Zhang, "Aerodynamics of a Heaving Airfoil in Ground Effect," *AIAA J.*, vol. 49, no. 6, pp. 1168–1179, Apr. 2011.

[3] R. De Breuker, R. De Breuker, M. Abdalla, M. Abdalla, A. Milanese, A. Milanese, P. Marzocca, and P. Marzocca, "Optimal Control of Aeroelastic Systems using Synthetic Jet Actuators," *Order A J. Theory Ordered Sets Its Appl.*, pp. 1–12, 2008.

[4] J. R. Wright and J. E. Cooper, *Introduction to Aircraft Aeroelasticity and Loads*. 2008.

[5] R. S. Floyd and E. H. Law, "Simulation and Analysis of Suspension and Aerodynamic Interactions of Race Cars," Dec. 1994.

[6] P. Aschwanden, J. Müller, and U. Knörnschild, "Experimental Study on the Influence of Model Motion on the Aerodynamic Performance of a Race Car," Apr. 2006.

[7] P. C. Murphy and V. Klein, "Estimation of Aircraft Unsteady Aerodynamic Parameters From Dynamic Wind Tunnel Testing," *AIAA Atmos. Flight Mech. Conf. Exhib. 6-9 August 2001, Montr. Canada*, pp. 1–9, 2001.

[8] S. Brunton and C. Rowley, "Low-dimensional state-space representations for classical unsteady aerodynamic models," *… Sci. Meet. Incl. new horizons …*, no. January, pp. 4–7, 2011.

[9] N. SATO, M. KAWAKAMI, Y. KATO, M. INAGAKI, and N. HORINOUCHI, "LES Analysis of Incompressible Flows around an

Automobile in Motion Using ALE Method (4th Report, Unsteady Aerodynamic Analysis around a Simplified Car Model in Pitch Motion),” *Trans. JAPAN Soc. Mech. Eng. Ser. B*, vol. 77, no. 773, pp. 43–55, 2011.

[10] S. Brunton, C. Rowley, and D. Williams, “Linear Unsteady Aerodynamic Models from Wind Tunnel Measurements,” *41st AIAA Fluid Dyn. Conf. Exhib.*, pp. 1–13, Jun. 2011.

[11] S. Cheng and M. Tsubokura, “A numerical analysis of transient flow past road vehicles subjected to pitching oscillation,” *J. Wind …*, 2011.

[12] H. Haddadpour and R. D. Firouz-Abadi, “Evaluation of quasi-steady aerodynamic modeling for flutter prediction of aircraft wings in incompressible flow,” *Thin-Walled Struct.*, vol. 44, no. 9, pp. 931–936, Sep. 2006.

[13] M. Sohail and R. Ullah, “CFD of Oscillating Airfoil Pitch Cycle by using PISO Algorithm,” *waset.org*, pp. 1929–1933, 2011.

[14] H. Sawamoto, T. Yasuki, H. Tanaka, and K. Ishii, “Unsteady Aerodynamic Analysis around Oscillating Ahmed body by LS-DYNA,” in *9th European LS-DYNA Conference*, 2013.

[15] M. Kawakami, N. Sato, P. Aschwanden, J. Mueller, Y. Kato, M. Nakagawa, and E. Ono, “Validation and Modeling of Transient Aerodynamic Loads Acting on a Simplified Passenger Car Model in Sinusoidal Motion,” Apr. 2012.

[16] M. Ariff, S. M. Salim, and S. C. Cheah, “Wall Y + Approach for Dealing With Turbulent Flow Over a Surface Mounted Cube : Part 2 – High Reynolds Number,” *Seventh International Conference on CFD in the Minerals and Process Industriesnd Process Industries*, 2009. [Online]. Available: http://www.cfd.com.au/cfd_conf09/PDFs/142SAL.pdf. [Accessed: 13-Mar-2015].

[17] C. Bak, P. L. Fuglsang, and J. Johansen, *Wind Tunnel Tests of the NACA 63-415 and a Modified NACA 63-415 Airfoil*, vol. 1193, no. December. 2000.

[18] S. L. Brunton, C. W. Rowley, and D. R. Williams, “Reduced-order unsteady aerodynamic models at low Reynolds numbers,” *J. Fluid Mech.*, vol. 724, pp. 203–233, Apr. 2013.

[19] C. O. Neill, “Aerodynamic System Identification MAE 6243 Project,” *System*, 2004. [Online]. Available: http://charles-oneill.com/projects/sifinal.pdf. [Accessed: 13-Mar-2015].

[20] L. Bernal and M. Ol, "Unsteady force measurements in pitching-plunging airfoils," *39th AIAA Fluid Dynamics …*, 2009. [Online]. Available: http://arc.aiaa.org/doi/pdf/10.2514/6.2009-4031. [Accessed: 13-Mar-2015].

[21] J. Molina, X. Zhang, and D. Angland, "On the unsteady motion and stability of a heaving airfoil in ground effect," *Acta Mech. Sin.*, vol. 27, no. 2, pp. 164–178, Apr. 2011.

[22] E. B. W. Victor L. Streeter, *Fluid Mechanics*. .

[23] H. Kowalczyk, "Damper Tuning with the use of a Seven Post Shaker Rig," *SAE Tech. Pap.*, vol. 2002–01–08, 2002.

[24] W. Milliken and D. Milliken, *Race car vehicle dynamics*. 1995.

[25] T. Cebeci, J. P. Shao, F. Kafyeke, and E. Laurendeau, "Computational fluid dynamics for engineers: from panel to Navier-Stokes methods with computer programs," 2005. [Online]. Available: http://books.google.com/books?id=37IHClTXkIEC&pgis=1. [Accessed: 13-Mar-2015].

[26] R. Aiguabella, "Formula One Rear Wing Optimization -," UPC Barcelona, 2011.

[1][2][3][4][5][6][7][8][9][10][11][12][13][14][15][16][17][18][19][20][21][22][23][24][25][26]